Hydrol. Earth Syst. Sci. Discuss., 12, 1653–1696, 2015
www.hydrol-earth-syst-sci-discuss.net/12/1653/2015/
doi:10.5194/hessd-12-1653-2015

Hydrology and Earth System Sciences
Open Access
Discussions

Spatially-distributed influence of agro-environmental factors governing nitrate fate and transport in an irrigated stream-aquifer system

R. T. Bailey[1], **M. Ahmadi**[2], **T. K. Gates**[1], **and M. Arabi**[1]

[1]Department of Civil and Environmental Engineering, Colorado State University, 1372 Campus Delivery, Fort Collins, CO, 80523-1372, USA
[2]Spatial Science Laboratory, Texas Agrilife Research, Texas A&M University, 1500 Research Plaza, College Station, TX 77843-2120, USA

Received: 9 December 2014 – Accepted: 10 January 2015 – Published: 4 February 2015

Correspondence to: R. T. Bailey (rtbailey@engr.colostate.edu)

Published by Copernicus Publications on behalf of the European Geosciences Union.

Abstract

Elevated levels of nitrate (NO_3) in groundwater systems pose a serious risk to human populations and natural ecosystems. As part of an effort to remediate NO_3 contamination in irrigated stream-aquifer systems, this study elucidates agricultural and environmental parameters and processes that govern NO_3 fate and transport at the regional (500 km^2), local (50 km^2), and field scales (< 1 km^2). Specifically, the revised Morris sensitivity analysis method was applied to a finite-difference nitrogen cycling and reactive transport model of a regional-scale study site in the Lower Arkansas River Valley in southeastern Colorado. The method was used to rank the influence of anthropogenic activities and natural chemical processes on NO_3 groundwater concentration, NO_3 mass leaching, and NO_3 mass loading to the Arkansas River from the aquifer. Sensitivity indices were computed for the entire study area in aggregate as well as each canal command area, crop type, and individual grid cells. Results suggest that fertilizer loading, crop uptake, and heterotrophic denitrification govern NO_3 fate and transport for the majority of the study area, while canal NO_3 concentration and rates of autotrophic denitrification, nitrification, and humus decomposition dominate or partially dominate in several canal command areas. Also, NO_3 leaching and groundwater concentration in adjacent cultivated fields often are governed by different processes and mass inputs/outputs. Results can be used to determine critical processes and key management actions for future data collection and remediation strategies, with efforts able to be focused on localized areas.

1 Introduction

During recent decades, elevated concentration of nitrate (NO_3) C_{NO_3} in groundwater systems and at points of groundwater discharge to surface water bodies has become a serious environmental issue due to its adverse effects on human populations and natural ecosystems (Spalding and Exner, 1993). Specific problems associated with high

HESSD
12, 1653–1696, 2015

C_{NO_3} include methemoglobinemia for infants (Fan and Steinberg, 1996) and eutrophication in aquatic systems, which induces depletion of dissolved oxygen (O_2) (hypoxia) due to increased biological activity. In addition, high C_{NO_3} can lead to elevated concentrations of sulfate and selenium (Se) via oxidation of pyrite (FeS_2) and seleno-pyrite ($FeSe_2$) from marine shale (Frind et al., 1990; Jørgensen et al., 2009; Bailey et al., 2012). NO_3 also has been shown to mobilize uranium via oxidation (Wu et al., 2010). Recent studies have revealed that certain rock formations can yield nitrogen (N) in response to a variety of biogeochemical processes (Holloway and Dahlgren, 2002; Montross et al., 2013). In most cases, however, elevated concentrations result from excessive loadings of organic or inorganic N fertilizer, inducing NO_3 leaching to the saturated zone of the aquifer (Korom, 1992; Spalding and Exner, 1993).

To combat NO_3 contamination, numerous field and modeling studies have been performed to quantify NO_3 fate and transport processes in soil-groundwater systems, identify baseline conditions of N sources and transport patterns, and investigate potential remediation strategies. For the latter, simulation models typically are used to predict the effect of land use and best-managements practices (BMPs) such as reduction in fertilizer loading (Chaplot et al., 2004; Almasri and Kaluarachchi, 2007; Lee et al., 2010), reduction in applied irrigation water (Ma et al.,1998; Rong and Xuefeng, 2011), and implementing or enhancing riparian buffer zones (Hefting and Klein, 1998; Spruill, 2000; Vaché et al., 2002; Sahu and Gu, 2009) on overall C_{NO_3} and on NO_3 mass loading to and within streams. These studies have been conducted at various scales (Ocampo et al., 2006), ranging from the soil profile and field scale (Johnsson et al., 1987; Ma et al., 1998; Rong and Xuefeng, 2011), to the catchment scale (Birkinshaw and Ewen, 2000; Conan et al., 2003; Wriedt and Rode, 2006; Lee et al., 2010), to the regional-scale watershed or river basin scale (Chaplot et al., 2004; Almasri and Kaluarachchi, 2007), and include a variety of fate and transport processes such as soil N cycling, leaching, groundwater transport, and overland transport.

Besides assessing baseline conditions and predicting domain-scale effects on spatial concentrations and loadings, numerical models also can be used in NO_3 remedi-

HESSD
12, 1653–1696, 2015

ation to determine the system inputs, parameters, and processes (i.e., model factors) that govern these concentrations and loadings. In general, identifying the most influential processes on resulting C_{NO_3} and mass loading can assist in establishing optimal remediation strategies. Additional benefits of the analysis include guiding effective field sampling strategies by focusing on influential system variables or inputs; facilitating model calibration and testing by focusing on the identified key factors (Sincock et al., 2003; Almasri and Kaluarachchi, 2007); identifying factors that require additional research to improve model performance (Hall et al., 2009); and detecting non-influential parameters or processes that possibly could be eliminated to simplify the model (Saltelli et al., 2008).

An appealing approach to determine the influence of model factors is sensitivity analysis (SA), which relates changes in model output variables (e.g., concentration, mass loading) to prescribed changes in model factor input values (e.g., initial conditions, system stresses, system parameters). For studies assessing NO_3 fate and transport in groundwater systems using physically-based spatially-distributed groundwater models, sensitivity analysis typically is performed in a simple fashion due to model complexity and computational cost. For example, Almasri and Kaluarachchi (2007) increased values of selected parameters (e.g., denitrification rate, longitudinal dispersivity, initial concentration, soil mineralization rate, soil nitrification rate, fertilizer loading) by 50 % to determine their influence on simulated C_{NO_3} in a watershed in Washington state, USA; Ehteshami et al. (2013), using the LEACHN model, investigated the influence of low and high values of rainfall and initial C_{NO_3} for two soil types on soil C_{NO_3}. In a field study using the RISK-N model, Oyarzun et al. (2007) modified values of soil initial N, C_{NO_3} in irrigation water, fertilizer, N crop uptake, crop evapotranspiration (ET), and soil properties by 50, 70, 100, 125, and 150 % to investigate their influence on NO_3 vadose zone mass flux and C_{NO_3} in the groundwater. Whereas global effect of the model factor on system-response variables can be assessed, local and interaction effects cannot be quantified.

HESSD
12, 1653–1696, 2015

A more rigorous SA method is global sensitivity analysis (GSA), which searches the entire parameter space to identify the importance of model parameters and interactions thereof. Such methods include the Elementary Effects (EE) method (Morris, 1991; Cacuci, 2003), a screening method that identifies the most important model factors and is well-suited for large models (Campolongo and Braddock, 1999), and variance-based methodsthat quantitatively decomposes the variance of model output into fractions that are attributed to model factors (Saltelli et al., 2008). A number of hydrologic modeling studies have used GSA methods for assessing model factor influence on overall watershed nutrient and sediment processes (White and Chaubey, 2005; Arabi et al., 2007; Sun et al., 2012; Ahmadi et al., 2014), flooding and hydraulic characteristics (Hall et al., 2005, 2009), and in-stream water quality (Cox and Whitehead, 2005; Deflandre et al., 2006; Liu and Zou, 2012; Bailey and Ahmadi, 2014).

Sensitivity analysis is commonly used in hydrologic and water quality modeling to identify the influence of model parameters on an aggregated measure of model responses such as average annual stream discharge or contaminant loads. A few studies have assessed how the results of SA vary in time. For example Reusser et al. (2011) used hydrologic catchment models to investigate the temporal-varying influence of model factors on a variety of watershed response variables for catchments in Ecuador and Germany. However, the spatial variability of sensitivity indices has been largely neglected. Specifically regarding this study, no studies have quantified the spatial-varying influence of factors on solute concentrations in large-scale groundwater systems. Such information could be valuable in terms of implementing site-specific remediation strategies, facilitating model calibration for specific model domain regions, and identifying system variables that require additional field data collection, particularly for NO_3 due to its ubiquitous presence in groundwater systems worldwide.

This study aims to identify the spatially-varying influence of system factors on NO_3 fate and transport in a regional-scale (506 km^2) irrigated hydro-agricultural system. Specifically, the factors' influence on NO_3 groundwater concentrations, NO_3 leaching below root zone, and NO_3 groundwater mass loading to the stream network will be

HESSD
12, 1653–1696, 2015

quantified for a variety of scales (cultivated field, canal command area, region). A calibrated and tested N fate and transport groundwater model is used for the assessment, with the modified Morris method used for the sensitivity analysis.

2 Methods

A comprehensive SA method was applied to a regional-scale, intensively irrigated 506 km^2 groundwater system in the Lower Arkansas River Valley (LARV) in southeastern Colorado to identify the spatially-varying influence of system factors on NO_3 concentrations in groundwater, NO_3 mass leaching in the shallow soil zone, and NO_3 mass loading to the Arkansas River. The model used is UZF-RT3D (Bailey et al., 2013a, b), a MODFLOW (Niswonger et al., 2011) based, finite-difference model designed for N fate and transport at the regional scale and recently calibrated and tested for the study area (Bailey et al., 2014). The model accounts for major agricultural inputs (fertilizer, canal seepage, irrigation water), processes (N cycling in the root and soil zone, leaching, three-dimensional transport, heterotrophic and autotrophic denitrification), and outputs (mass loading to the stream network).

As identifying the relative importance of parameters and processes in space is the objective of this study, and since computational costs of UZF-RT3D are extremely high (run-time of approximately 3.5 h for a single simulation using an Intel® Core™ i7-3770 CPU @ 3.40 GHz desktop computer), the SA method used is an improved variant (Campolongo et al., 2007) of the Morris method (Morris, 1991) rather than variance-based SA methods such as Sobol' (Sobol', 1993) or FAST (Fourier Amplitude Sensitivity Test) (Cukier et al., 1973). Nine model factors are included in the assessment. In conjunction with the SA methodology, model results are processed to determine the dominant model factors globally (i.e., averaged for the entire model domain), for each irrigation canal command area, for each crop type (i.e., the set of model grid cells associated with each crop type), and for each grid cell, thereby elucidating parameter influence at varying spatial scales. For the latter, spatial contour maps depicting model

HESSD
12, 1653–1696, 2015

sensitivity to individual model factors are shown. Due to the dependence of N fate and transport on the presence of O_2, the influence of the 9 model input factors on C_{O_2} also is calculated and presented.

2.1 Study area

The LARV in Colorado extends from the outlet of the Arkansas River from Pueblo Reservoir eastward across southeastern Colorado to the border with Kansas (Fig. 1), with the Arkansas River fed primarily by snowmelt from the mountainous regions of the upper Arkansas basin. The climate is semi-arid, with average monthly precipitation and monthly temperatures ranging from 0.7 cm and −1 °C during the winter months, respectively, to 5.0 cm and 25 °C during the summer months. In total, the valley supports approximately 109 000 irrigated ha (270 000 ac), with more than 1600 km of main earthen canals and 2400 pumping wells, and is one of the most productive agricultural areas for the state of Colorado. The irrigation season begins in mid-March and ends in early November, with water diverted from the Arkansas River into canals. Approximately 14 000 fields are cultivated, with the majority using flood irrigation methods and a small minority using sprinklers or drip irrigation methods. Major crops include alfalfa, corn, grass hay, wheat, sorghum, dry beans, cantaloupe, watermelon, and onions. Melons and onions are the principal cash crops.

The region of the LARV focused on in this study is shown in Fig. 1. The boundary of the study area is shown with a black line, and encompasses an area of 50 600 ha (125 000 ac), of which 26 400 ha (65 300 ac) are irrigated. Irrigation water is derived from the following six main canals: Rocky Ford Highline, Rocky Ford, Catlin, Fort Lyon, Holbrook, and Otero. The fields receiving water from each of these canals (i.e. canal command areas) are shown in Fig. 2a, with crop type cultivated in 2006 for each field shown in Fig. 2b. Due to over-irrigation and poor subsurface drainage, high water table elevations have been established in recent decades, with water table depth below ground surface often between 1–3 m (Morway and Gates, 2012). These high water tables have resulted in salinization and waterlogging, in addition to substantial rates

HESSD
12, 1653–1696, 2015

of groundwater return flows (i.e. discharge) to the Arkansas River and its tributaries (Morway et al., 2013). Referring to Fig. 1, Timpas Creek and Crooked Arroyo, in the southern portion of the region, are fed primarily from groundwater flow originating from adjacent irrigated fields. The thickness of the alluvial aquifer ranges from 4 to 34 m (Fig. 3a), and is underlain by Cretaceous Shale (Pierre Shale, Niobrara Shale, Carlisle Shale, Graneros Shale) (Scott, 1968; Sharps, 1976) in both solid and weathered form.

In addition to salinization and associated decrease in crop productivity (Morway and Gates, 2012), elevated groundwater C_{NO_3} has been observed, presumably due to over-fertilization on cultivated fields. In a similar irrigated region of the LARV, located about 67 km upstream, Zielinski et al. (1997) examined δ^{15}N isotopic signatures to conclude that NO_3 was derived primarily from fertilizer and crop waste, not from proximate geologic sources. To assess the C_{NO_3} in space and time in the study region, groundwater and surface water samples were collected from observation wells and surface water monitoring points (see locations in Fig. 2a) during 10 sampling events over the period 2006–2009, as described and summarized in Gates et al. (2009). For groundwater, samples were taken routinely from 52 observation wells, with groundwater from 37 additional observation wells sampled non-routinely (aperiodic). Surface water samples were taken from 10 locations along the Arkansas River and 5 locations in tributaries. Detailed results of the monitoring scheme are shown in Supplement. In summary, for groundwater the 85th percentile values of C_{NO_3-N} were at or in excess of the 10 mg L^{-1} (85th percentile) EPA drinking water standard for the first three sample trips. The maximum measured value was 66 mg L^{-1}. The mean for the samples gathered from the 10 sites along the Arkansas River was 1.53 mg L^{-1} and the mean for samples from tributaries was 1.95 mg L^{-1}. The annual median values of the Arkansas River samples were 0.95, 1.20, 1.10, and 2.20 mg L^{-1} for each of the successive years within the period 2006–2009, compared to the Colorado interim standard of 2 mg L^{-1} (CDPHE, 2012) for total N concentration ($C_{NO_3-N} + C_{NO_2-N} + C_{NH_4-N}$)in warm rivers and streams. The concentration of C_{NO_3-N} exceeded 2 mg L^{-1} in about 25 % of the samples gathered in the river over this period and exceeded 2.5 mg L^{-1} in about 12 % of the samples, sig-

HESSD
12, 1653–1696, 2015

nifying the growing concern about N pollution in the river. Analysis of 22 river samples and 15 tributary samples in 2013 revealed that C_{NO_3-N} made up greater than 80 % of total dissolved N in the river and about 76 % of total dissolved N in the tributaries.

Recently, an N cycling and reactive transport model (Bailey et al., 2014) was constructed, calibrated, and tested for the study region, in conjunction with Se cycling and reactive transport. A detailed description of the finite-difference numerical model is presented in Sect. 2.2. The model is linked with a MODFLOW-NWT (Niswonger et al., 2011) model also recently calibrated and tested for the study region (Morway et al., 2013), which uses the UZF1 unsaturated-zone flow package (Niswonger et al., 2006). The model uses horizontal cell dimensions of 250 m by 250 m (Fig. 3b), comparable to dimensions of cultivated fields. Weekly infiltrated irrigation water, calculated from estimated applied water volume and tail water runoff, is based on crop type and the recorded volumes of diverted canal water from the Arkansas River (Morway et al., 2013). Timing of water application to the fields is based on a hierarchy of crop demand, according to the following order: onions, peppers and tomatoes, melons, pumpkins and squash, alfalfa and corn, and so forth. Precipitation, canal seepage, crop ET, and groundwater-surface water interactions are also included. The model was run for the years 1999–2009 using weekly time steps, and was tested against observations of water table elevation, groundwater return flow to the stream network, recharge to infiltration ratios, canal seepage, total ET, and irrigation flows. Figure 2b–d show the finite-difference grid, the simulated water content of the soil in June 2006, and the average simulated water table elevation (m) during the 1999–2009 time period, respectively.

2.2 UZF-RT3D N reaction module and baseline application

UZF-RT3D simulates the reactive transport of multiple interacting chemical species in variably-saturated porous media using groundwater flow rates, water content, and a variety of groundwater sources and sinks (e.g., applied irrigation water, pumping, canal seepage, groundwater-surface water interactions) simulated by a MODFLOW-NWT model using the UZF1 package. The N cycling and reaction module add-on

HESSD
12, 1653–1696, 2015

package (Bailey et al., 2013b) was designed for model application in an irrigated agricultural groundwater system, and accounts for the major hydrologic, chemical, and land management processes that govern N fate and transport in an irrigated stream-aquifer system. Also, due to the dependence of N cycling and transport on the presence of O_2, the fate and transport of O_2 is included.

A schematic of the fate and transport of N species and O_2 as simulated by the N reaction module of UZF-RT3D is depicted in Fig. 4a. N mass (NO_3 or NH_4) enters the subsurface via fertilizer loading (single application or split application), canal seepage, infiltrating irrigation water (either from canal water or pumped groundwater), or seepage from the stream network (Arkansas River and its tributaries). N mass exits the subsurface via groundwater discharge to the stream network. N cycling occurs in the root and soil zone, with organic N and carbon (C) added to soil organic matter (manure M_N, fast-decomposing litter L_N, flow-decomposing humus H_N) via after-harvest plowing or decaying root mass and subsequently mineralized to NH_4, which can be volatilized, nitrified to NO_3, or take up with NO_3 into crop roots during the growing season. The timing of land management actions, e.g. fertilizer loading (40, 60 % split application), irrigation events, harvesting, and plowing, adopted in the module is shown in Fig. 4b. NH_4 is sorbed readily to soil surface sites, whereas NO_3 is transported by one-dimensional transport in the unsaturated zone and three-dimensional transport in the saturated zone, subject to heterotrophic denitrification in near-surface areas and autotrophic denitrification in the presence of marine shale (see Fig. 1). O_2 also is subject to heterotrophic and autotrophic chemical reduction. The stoichiometry of the reaction for autotrophic reduction of O_2 and NO_3 in the presence of FeS_2-bearing shale (see Fig. 4a) are:

$$2FeS_2 + 7O_2 + 2H_2O \rightarrow 2Fe^{2+} + 4SO_4^{2-} + 4H^+ \quad \text{(R1)}$$

$$5FeS_2 + 14NO_3^- + 4H^+ \rightarrow 5Fe^{2+} + 10SO_4^{2-} + 7N_2 + 2H_2O \quad \text{(R2)}$$

UZF-RT3D solves a system of advection-dispersion-reaction (ADR) equations for interacting dissolved-phase and solid-phase species using the finite-difference approach.

HESSD
12, 1653–1696, 2015

Including ADR processes and source/sink terms as depicted, the following mass conservation equations are written for the dissolved-phase species (NO_3, NH_4, O_2) in the N reaction module:

$$\frac{\partial\left(C_{\mathrm{NH_4}}\theta\right)}{\partial t}R_{\mathrm{NH_4}} = -\frac{\partial}{\partial x_i}\left(\theta v_i C_{\mathrm{NH_4}}\right) + \frac{\partial}{\partial x_i}\left(\theta D_{ij}\frac{\partial C_{\mathrm{NH_4}}}{\partial x_j}\right) + q_{\mathrm{f}}C_{f_{\mathrm{NH_4}}} + F_{\mathrm{NH_4}} - U_{\mathrm{NH_4}} + \varepsilon\left(r_{\mathrm{s,N}}^{\mathrm{min}} - r_{\mathrm{s,N}}^{\mathrm{imm}}\right) + \theta\left(-r_{\mathrm{f}}^{\mathrm{nit}} - r_{\mathrm{f}}^{\mathrm{vol}}\right) \quad (1)$$

$$\frac{\partial\left(C_{\mathrm{NO_3}}\theta\right)}{\partial t} = -\frac{\partial}{\partial x_i}\left(\theta v_i C_{\mathrm{NO_3}}\right) + \frac{\partial}{\partial x_i}\left(\theta D_{ij}\frac{\partial C_{\mathrm{NO_3}}}{\partial x_j}\right) + q_{\mathrm{f}}C_{f_{\mathrm{NO_3}}} + F_{\mathrm{NO_3}} - U_{\mathrm{NO_3}} + \theta\left(r_{\mathrm{f}}^{\mathrm{nit}} - r_{\mathrm{f,NO_3}}^{\mathrm{het}} - r_{\mathrm{f,NO_3}}^{\mathrm{auto}}\right) \quad (2)$$

$$\frac{\partial\left(C_{\mathrm{O_2}}\theta\right)}{\partial t} = -\frac{\partial}{\partial x_i}\left(\theta v_i C_{\mathrm{O_2}}\right) + \frac{\partial}{\partial x_i}\left(\theta D_{ij}\frac{\partial C_{\mathrm{O_2}}}{\partial x_j}\right) + q_{\mathrm{f}}C_{f_{\mathrm{O_2}}} + \theta\left(-r_{\mathrm{f,O_2}}^{\mathrm{het}} - r_{\mathrm{f,O_2}}^{\mathrm{auto}}\right) \quad (3)$$

where C is solute concentration [$M_f L_f^{-3}$], with f denoting fluid phase; v is the pore velocity [$L_b T^{-1}$], provided by MODFLOW-UZF1; θ is the volumetric water content [$L_f^3 L_b^{-3}$], also provided by MODFLOW-UZF1; D_{ij} is the hydrodynamic dispersion coefficient [$L^2 T^{-1}$]; q_f is the volumetric flux of water representing sources and sinks [$L_f^3 T^{-1} L_b^{-3}$] such as irrigation water, canal and river seepage, groundwater discharge to the river, or pumped groundwater, with b denoting the bulk phase; C_f is the concentration of the source or sink [$M_f L_f^{-3}$]; F is the inorganic fertilizer application [$M_f L_b^{-3} T^{-1}$]; U is the potential crop uptake rate [$M_f L_b^{-3} T^{-1}$]; ε is the volumetric solid content [$L_s^3 L_b^{-3}$] with s denoting the solid phase, and is equal to $1 - \phi$, where ϕ is porosity [$L_f^3 L_b^{-3}$]; r_f represents the rate of all reactions that occur in the dissolved-phase [$M_f L_f^{-3} T^{-1}$]; min, imm, nit, and vol signify mineralization, immobilization, nitrification, and volatilization of NH_4,

HESSD
12, 1653–1696, 2015

respectively; and auto and het represent autotrophic and heterotrophic chemical reduction, respectively. ε is included for the min and imm reactions to denote a mass transfer between the solid and dissolved phases. For NH_4, which is subject to sorption, R is the retardation factor and is equal to $1 + (\rho_b K_{d,NH_4})/\theta$, where ρ_b is the bulk density of the porous media [$M_b\,L_b^{-3}$] and K_{d,NH_4} is the partitioning coefficient [$L_f^{-3}\,M_b$]. The daily mass of potential N crop uptake during the growing season is determined using a logistic equation (Johnsson et al., 1987) and is distributed across the vertical column of grid cells encompassing the crop rooting depth according to the mass density of the root system.

The rate of chemical reactions r_f included in Eqs. (1)–(3) is governed by the dependence of the chemical reaction on soil temperature T, θ, and the presence of O_2 and C. These rates are simulated using first-order Monod kinetics, with the following rate law expressions established for nitrification of NH_4, volatilization of NH_4, and heterotrophic and autotrophic reduction of O_2 and NO_3:

$$r_f^{nit} = \lambda^{nit} C_{NH_4} E \tag{4}$$

$$r_f^{nit} = \lambda^{vol} C_{NH_4} E \tag{5}$$

$$r_{f,O_2}^{het} = \lambda_{O_2}^{het} C_{O_2} \left(\frac{C_{O_2}}{K_{O_2} + C_{O_2}}\right)\left(\frac{CO_{2,prod}}{K_{CO_2} + CO_{2,prod}}\right) E \tag{6}$$

$$r_{f,NO_3}^{het} = \lambda_{NO_3}^{het} C_{NO_3} \left(\frac{C_{NO_3}}{K_{NO_3} + C_{NO_3}}\right)\left(\frac{CO_{2,prod}}{K_{CO_2} + CO_{2,prod}}\right)\left(\frac{I_{O_2}}{I_{O_2} + C_{O_2}}\right) E \tag{7}$$

$$r_{f,O_2}^{auto} = \lambda_{O_2}^{auto} C_{O_2} \left(\frac{C_{O_2}}{K_{O_2} + C_{O_2}}\right) \tag{8}$$

$$r_{f,NO_3}^{auto} = \lambda_{NO_3}^{auto} C_{NO_3} \left(\frac{C_{NO_3}}{K_{NO_3} + C_{NO_3}}\right)\left(\frac{I_{O_2}}{I_{O_2} + C_{O_2}}\right) \tag{9}$$

HESSD
12, 1653–1696, 2015

where λ is the base rate constant for the reaction [T^{-1}]; K_j is the Monod half-saturation constant for species j [$M_f L_f^{-3}$]; I_{O_2} is the O_2 inhibition constant [$M_f L_f^{-3}$] signifying the species concentration at which lower-redox species can undergo appreciable rates of reduction; $CO_{2,prod}$ is the total mass of CO_2 produced during organic matter decomposition and is used as an indicator of available OC for microbial consumption (Birkinshaw and Ewen, 2000); and E [–] is an environmental reduction factor that accounts for θ and T and acts to temper the reaction rates based on microbial activity (Birkinshaw and Ewen, 2000; Bailey et al., 2013b).

Mass conservation equations (not shown) for solid-phase organic N (and C) species L_N, H_N, and M_N also are implemented, following Johnsson et al. (1987) and Birkinshaw and Ewen (2000) and the schematic in Fig. 4a, similar to the mass conservation equations shown for organic Se species in Bailey et al. (2013b). Root and stover mass is added to the soil organic matter. Decomposed organic N mass is transferred to H_N and L_N through incorporation of microbial biomass or, if there is any remaining, to NH_4 via mineralization. If the requirement of N mass for microbial growth in soil organic matter is not satisfied, NH_4 mass is immobilized to organic N.

The baseline N reactive transport model used in this study for sensitivity analysis is the same as that described in Bailey et al. (2014), with the same model domain and finite difference grid as the groundwater flow model (see Fig. 3b). The model has 7 vertical layers, with Layers 1–2 (0.5 m each) corresponding to the root zone, Layer 3 (1.0 m) corresponding to the leaching zone, Layers 4–6 to the saturated zone, and Layer 7 to the shale bedrock formation. Each vertical column of cells in the 3-D grid is assigned a set of crop parameter values according to the portions of fields within the grid cell area. Crop parameters, with values shown in Table 1 for each crop type in the study area, include: Planting Day; Harvest Day; Plowing Day; mass of stover plowed into the soil P_{St} (kg ha^{-1}) after harvest; maximum rooting depth $d_{rt,\,max}$ (m), which controls N uptake; C-N ratio of root mass CN_{RT}; fertilizer loading F_{NH_4} (kg ha^{-1}), maximum seasonal uptake values of N N_{up} (kg ha^{-1}), depth of plowing d_{pw} (m); mass

HESSD
12, 1653–1696, 2015

of decaying roots P_{Rt} (kg ha^{-1}); C-N ratio of stover mass CN_{ST}; and constants defining root growth and daily uptake rate U. Chemical reaction parameter values are shown in Table 2, with an asterisk * indicating the mean value of all the grid cells. C_{NO_3} and C_{O_2} of canal water and irrigation water were based on observed data. The model was run for the 2006–2009 and tested against spatio-temporal averages of groundwater C_{NO_3} and NO_3 mass loadings from the aquifer to the Arkansas River.

2.3 Application of the Morris Sensitivity Analysis method

2.3.1 Morris SA methodology

The Morris screening method for global SA is based on an individually randomized one-at-a-time (OAT) design that provides information regarding (i) the main effect of each input parameter on model output responses and (ii) the overall effects including interactions between parameters. For example, consider a model M with a vector of k parameters (θ_i, $i = 1, \ldots, k$) within the feasible parameter space, Θ, that simulates m response vectors of the system (S_j, $j = 1, \ldots, m$):

$$[S_1, \ldots, S_m] = M(\theta_1, \ldots, \theta_k) \tag{10}$$

Similar to any standard SA practice, parameters are drawn from their predefined distributions, with each model input parameter θ_i varied across p discrete values (Saltelli et al., 2008). After running model M for the given parameter sets, the local sensitivity measure (also referred to as the *elementary effect*, EE) is then computed for each parameter i for model response j as follows:

$$\mathrm{EE}_{i,j}(\theta) = \left(\frac{S_j(\theta_1, \ldots, \theta_{i-1}, \theta_i + \Delta, \ldots \theta_k) - S_j(\theta)}{\Delta} \right) \tag{11}$$

where Δ is a value in the predefined increments (i.e. $[1/(p-1), \ldots, 1 - 1/(p-1)]$) and $\theta = \theta_1, \ldots, \theta_k$ is a random sample in the parameter space so that the transformed point

HESSD
12, 1653–1696, 2015

$(\theta_1, \ldots, \theta_{i-1}, \theta_i + \Delta, \ldots \theta_k)$ is still within the parameter space Θ (Saltelli et al., 2008). The resulting distribution EE_i associated with each parameter θ_i is then analyzed to determine μ, the mean of the distribution which assesses the overall importance of the parameter on the model output; and σ, the SD of the distribution, which indicates non-linear effects and/or interactions (Campolongo et al., 2007). A high value of σ for the EE distribution signifies that the value of θ_i chosen in a given simulation has a strong influence on the resulting EE value, hence indicating that the effect of the parameter on model output is strongly dependent on the values of the other parameters. A low value of σ signifies that the EE value is almost the same given any value of θ_i in the simulation, indicating a linear relationship between θ_i and the model output and that the effect of θ_i is independent of the values assigned to other parameters.

To determine sensitive and insensitive values, it is recommended to evaluate a graphical representation of σ vs. μ. However, for non-monotonic models, some EE values with opposite signs may cancel out when μ is calculated, and hence Campolongo and Saltelli (1997) proposed the use of μ^*, the sample mean of distribution of absolute values of EE. μ^* includes all types of effects that parameters can have on output responses and, therefore, is a global measure of output sensitivity to the parameters (Campolongo et al., 2007). $\mu^*_{i,j}$ is defined as the mean of absolute values of the computed elementary effects $EE_{i,j}$. The total computational cost of the Morris experiment is $n = r(k+1)$ runs, where r is the selected size of each sample.

As noted above, an important objective of SA is to determine the most influential model input parameters. Hence, it is important to measure the level of agreement between results of SA experiments with an emphasis on the high-ranked parameters. Campolongo and Saltelli (1997) suggested the use of the Savage score to facilitate comparison of results from different SA experiments (see next section). The Savage score is defined as follows (Iman and Conover, 1987):

$$SS_i = \sum_{h=i}^{k} \frac{1}{h} \tag{12}$$

HESSD
12, 1653–1696, 2015

where i is the rank assigned to the ith model parameter based on the Morris μ^*. The Savage score can be used in aggregating the results from different SA methods.

2.3.2 Model input factors analyzed

In applying the SA method to the UZF-RT3D model of the study area, 9 model input factors were analyzed for impact on model results: F_{NH_4}, N_{up}, C_{NO_3} in canal water $Canal_{NO_3}$, rate of litter pool decomposition λ_L, rate of humus pool decomposition λ_H, rate of autotrophic reduction of O_2 in the presence of shale $\lambda_{O_2}^{auto}$, rate of autotrophic reduction of NO_3 in the presence of shale $\lambda_{NO_3}^{auto}$, rate of nitrification λ_{nit}, and rate of heterotrophic denitrification $\lambda_{NO_3}^{het}$. $Canal_{NO_3}$ conveys NO_3 mass into the subsurface system via applied irrigation water as well as seeped canal water. For each simulation, separate values of F_{NH_4} and N_{up} were generated for each crop type, separate values of $Canal_{NO_3}$ were generated for each of the six canal command areas, and separate values of $\lambda_{O_2}^{auto}$, $\lambda_{NO_3}^{auto}$, and λ_{nit} were generated for each command area. The mean of each parameter value is derived from the baseline simulation (see Tables 1 and 2), with the mean values of $\lambda_{O_2}^{auto}$, $\lambda_{NO_3}^{auto}$, and λ_{nit} for each command area estimated during the calibration phase (Bailey et al., 2014).

Setting the number of replications r and levels p of the Morris scheme to 20 and 10, respectively, a total of 280 simulations were run. Parameter values were perturbed using a coefficient of variation (CV) of 0.2 for all parameters except for $Canal_{NO_3}$, which was perturbed with a CV of 0.1 based on variance in observed canal water concentrations. Perturbation for the reaction rates (λ_L, λ_H, $\lambda_{O_2}^{auto}$, $\lambda_{NO_3}^{auto}$, $\lambda_{NO_3}^{het}$, λ_{nit}) was performed using log values since statistically these rates typically conform to a lognormal distribution (Parkin and Robinson, 1989; McNab and Dooher, 1998). CV values were selected by comparing the resulting spread of parameter values to values found in the literature and from field data in the study area. The values of F_{NH_4}, $\lambda_{NO_3}^{auto}$, and $Canal_{NO_3}$ for each of the 280 simulations are shown in Fig. 5, with averages of 250 kg ha^{-1},

HESSD
12, 1653–1696, 2015

1.055×10^{-4} day^{-1}, and 2.6 g m^{-3}, respectively. The values shown in Fig. 5a are for grid cells that contain corn, and the values shown in Fig. 5b and c are for the grid cells within the Rocky Ford Highline canal command area (canal feeding the gray-shaded fields in Fig. 2a).

For each of the 280 simulations, the model was run for a 2 year spin-up period, followed by the 2006–2009 period. Model results were processed to determine the influence of the 9 targeted model input factors on groundwater C_{NO_3}, NO_3 mass leached from the root zone, and total NO_3 mass loading to the Arkansas River from the aquifer. Post-processing was implemented to determine this influence (i) globally for the entire study area, i.e. averaging values from all grid cells; (ii) for individual crop types, i.e. averaging values from all grid cells corresponding to a given crop type; (iii) for individual canal command areas, i.e. averaging values from all grid cells within a given command areas; and (iv) for individual grid cells. As total NO_3 mass loading to the Arkansas River occurs along the entire reach of the river within the study area, parameter influence is assessed only for (i). Values of average concentration, average leaching, and total mass loading were processed from the final year of the model simulation (i.e. 2009). For groundwater C_{NO_3}, concentration values were taken from Layer 4 of the model, which corresponds to the depth of observation well screens. For NO_3 leaching, values are taken from Layer 3 (i.e. the mass leached from Layer 3 to Layer 4). For parameter influence on C_{NO_3} for individual grid cells (item iv), the Savage score as calculated by Eq. (12) will be used for presentation of results. Also for (iv), the parameter influence on C_{O_2} will be presented.

3 Results and discussion

3.1 General model results

Model results from one of the 280 simulations is shown in Fig. 6, with spatial distribution of C_{O_2} and C_{NO_3} shown in Fig. 6a and b, respectively for 22 July 2009, and the

HESSD
12, 1653–1696, 2015

spatial distribution of NO_3 mass loading shown for one week during the winter (2 December 2006, Fig. 6c) and one week during the summer (10 August 2008, Fig. 6d). Mass loadings from the aquifer to the stream network (discharge) are displayed in red, whereas loadings from the stream network to the aquifer (seepage) are displayed in green. For concentrations in groundwater, values of C_{O_2} range from 0.0 to 10.3 mg L^{-1}, with an average value of 2.7 g m^{-3} for the 7776 active grid cells. Values of C_{NO_3} range from 0.0 to 78.3 mg L^{-1}, with an average value of 1.84 mg L^{-1}. Hotspots occur for both C_{O_2} and C_{NO_3}, with those of C_{NO_3} typically occurring in locations of corn cultivation due to the higher loading of F_{NH_4} as compared to other crop types. NO_3 mass loadings occur along the Arkansas River and the tributaries, with discharge and seepage both occurring along the length of the canals during the summer (Fig. 6d). The spatio-temporal average value of C_{NO_3} in groundwater for each command area during the entire 2006–2009 time period is shown in Fig. 7 for each of the 280 simulations. The average value for all grid cells in non-cultivated area also is shown. For all simulations, average C_{NO_3} for the Highline, Otero, Catlin, Rocky Ford, Fort Lyon, Holbrook, and non-cultivated areas is 2.0, 0.8, 1.4, 1.5, 3.7, 1.9, and 3.5 mg L^{-1}, respectively.

3.2 Parameter influence on global concentration, leaching, and loading of NO_3

The global influence of the 9 model input factors on NO_3 fate and transport in the study area is shown in Fig. 8. Global sensitivity plots are used, with non-linear effects and/or interactions σ plotted against mean μ^*. The influence of the factors on C_{NO_3} in Layer 1 (top 0.5 m of the root zone), C_{NO_3} in Layer 4 (shallow saturated zone), NO_3 leaching from Layers 3 to 4 $L_{NO_3Lay3\rightarrow4}$ (generally from the unsaturated zone to the saturated zone), and total NO_3 mass loading to the Arkansas River $Load_{NO_3}$ are shown in Fig. 8a–d, respectively. As seen in Fig. 8a, C_{NO_3} in the root zone is governed principally by F_{NH_4} and N_{up} and to a smaller degree by $\lambda^{het}_{NO_3}$ and λ_{nit}. In the shallow saturated zone (Fig. 8b), where NO_3 mass is received from the upper soil zone via leaching, F_{NH_4}

HESSD
12, 1653–1696, 2015

and N_{up} still are dominant, but $Canal_{NO_3}$ has a stronger direct impact than $\lambda^{het}_{NO_3}$. The rate of humus decomposition, λ_H, and $\lambda^{auto}_{NO_3}$ also have a slight impact. NO_3 leaching also is governed by F_{NH_4}, N_{up}, $\lambda^{het}_{NO_3}$, $Canal_{NO_3}$, and λ_H (Fig. 8c), as higher F_{NH_4}, lower N_{up}, lower $\lambda^{het}_{NO_3}$, and higher $Canal_{NO_3}$ increase the mass of NO_3 leached, and vice versa. $Load_{NO_3}$ is governed by F_{NH_4}, N_{up}, and $\lambda^{het}_{NO_3}$ (Fig. 8d), with $\lambda^{het}_{NO_3}$ influencing not only how much NO_3 is leached to the water table and carried to the stream network via groundwater flow, but also how much NO_3 undergoes denitrification in the riparian areas of the stream network.

The high σ values for N_{up}, F_{NH_4}, $\lambda^{het}_{NO_3}$ and $Canal_{NO_3}$ shown in Fig. 8 signify the large spread in EE values for these parameters, indicating that their influence on C_{NO_3}, NO_3 leaching, and NO_3 mass loading is strongly dependent on the values of other parameters. For example, in reference to C_{NO_3} in the shallow saturated zone (Fig. 8b), the value of μ^* for N_{up} signified the average effect of N_{up} on C_{NO_3}, but some values of EE for N_{up} were much smaller and larger than μ^*. Smaller values of EE indicate that the combined influence of other parameter values produced a small effect of N_{up} on C_{NO_3}, such as a lower value of F_{NH_4} and a higher value of $\lambda^{het}_{NO_3}$, whereas larger values indicate that the combined influence of other parameters produced a larger effect of N_{up} on C_{NO_3}, such as a higher value of F_{NH_4} and a lower value of $\lambda^{het}_{NO_3}$. Larger values of $Canal_{NO_3}$ also would increase the influence of N_{up} on C_{NO_3}, as more NO_3 mass is brought into the soil zone via canal seepage or infiltrating irrigation water. Results suggest that first, detailed field sampling and observation of F_{NH_4}, N_{up}, $\lambda^{het}_{NO_3}$ and $Canal_{NO_3}$ must be performed as often as possible to provide accurate model input data; and second, these input/output factors must be controlled via implemented management practices if C_{NO_3}, NO_3 leaching, and NO_3 mass loading to the Arkansas River are expected to decline in future decades, whereas other processes (organic N decomposition via λ_L, λ_H; nitrification of NH_4 via λ_{nit}) are not as important as target factors.

HESSD
12, 1653–1696, 2015

3.3 Parameter influence on C_{NO_3} and leaching for each crop type

The influence of each of the 9 parameters on C_{NO_3} in the shallow groundwater zone and on NO_3 leaching for each crop type in the study area is summarized in Tables 3 and 4, respectively using values of μ^*. The μ^* values of the 3 most influential parameters for each crop type are bolded. For the majority of crop types, C_{NO_3} in the shallow groundwater zone is governed by F_{NH_4}, N_{up}, and $\lambda^{het}_{NO_3}$ (Table 3), similar to the global analysis presented in Sect. 3.2. For example, μ^* for F_{NH_4}, N_{up}, and $\lambda^{het}_{NO_3}$ is 0.94, 0.72, and 0.30, respectively, for corn-cultivated areas, and 0.84, 0.81, and 0.28 for sorghum-cultivated areas. The exception is areas that cultivate onion, in which $Canal_{NO_3}$ ($\mu^* = 0.45$) ranks in the top three behind F_{NH_4} (1.21) and N_{up} (0.99). For many of the crops, λ_H and λ_{nit} have a small to moderate influence, whereas λ_L, $\lambda^{auto}_{O_2}$, and $\lambda^{auto}_{NO_3}$ have a negligible to small influence on C_{NO_3}.

The influence of the 9 parameters on NO_3 mass leaching to the shallow saturated zone (Table 4) follows the same pattern as for their influence on C_{NO_3}, with F_{NH_4}, N_{up}, and $\lambda^{het}_{NO_3}$ dictating the amount of NO_3 leached to the water table (values in boxes) and $Canal_{NO_3}$, λ_H, λ_{nit}, and λ_L having small to moderate values of μ^*. For corn-cultivated areas, the average effect μ^* of F_{NH_4}, N_{up}, and $\lambda^{het}_{NO_3}$ is 486.3, 366.8, and 172.3, respectively, compared to 51.3 for λ_H, 41.3 for $Canal_{NO_3}$, and 26.4 for λ_L, with 15.2, 1.0, and 0.2 for λ_{nit}, $\lambda^{auto}_{NO_3}$, and $\lambda^{auto}_{O_2}$, respectively. Again, $Canal_{NO_3}$ is the third most influential parameter for onion-cultivated areas, with $\mu^* = 1.6$, compared to 9.7 and 7.2 for F_{NH_4} and N_{up}, respectively. Results suggest that F_{NH_4}, N_{up}, and $\lambda^{het}_{NO_3}$ must be controlled to decrease C_{NO_3} and NO_3 mass leaching for each crop type, with $Canal_{NO_3}$ controlled to lower these values for onion-cultivated areas.

HESSD
12, 1653–1696, 2015

3.4 Parameter influence on C_{NO_3} and leaching in individual canal command areas

Summaries of the influence of each of the 9 parameters on C_{NO_3} in the shallow groundwater zone and on NO_3 leaching for each canal command area also are given in Tables 3 and 4. The results show importance differences between the command areas, with a mixture of F_{NH_4}, N_{up}, λ_{nit}, $\lambda^{het}_{NO_3}$, $\lambda^{auto}_{NO_3}$, and $Canal_{NO_3}$ providing noteworthy impacts on C_{NO_3} and NO_3 mass leaching. For influence on C_{NO_3} (Table 3), the top three influential parameters within the Catlin command area are N_{up} ($\mu^* = 0.26$), λ_{nit} (0.16), and F_{NH_4} (0.12), whereas the top three for the Rocky Ford command area are $Canal_{NO_3}$ (0.51), $\lambda^{auto}_{NO_3}$ (0.20), and N_{up} (0.15), with the strong influence of $\lambda^{auto}_{NO_3}$ due to the presence of outcropped shale in the command area and hence locations of autotrophic denitrification. $\lambda^{auto}_{NO_3}$ also has a strong influence in the Holbrook command area, with the third highest value of μ^* (0.11). $Canal_{NO_3}$ is ranked 3rd or higher in terms of μ^* in 3 of the 6 command areas (Rocky Ford, Otero, Highline). F_{NH_4}, N_{up}, and $\lambda^{het}_{NO_3}$ govern NO_3 mass leaching for each of the command areas (Table 4) except for the Catlin command area, in which λ_{nit} is ranked second ($\mu^* = 38.0$) and the Rocky Ford Ditch, in which $Canal_{NO_3}$ is ranked first ($\mu^* = 30.3$). Thus, similar to the crop-specific influence, F_{NH_4} and N_{up} must be managed to decrease decrease C_{NO_3} and NO_3 mass leaching in the majority of command areas. However, nitrification of NH_4 is an important control for the Catlin command area, $Canal_{NO_3}$ is important for the Highline, Otero, and Rocky Ford command areas, heterotrophic denitrification is important for each command area except Catlin and Rocky Ford Ditch, and autotrophic denitrification is important for the Holbrook and Rocky Ford Ditch command areas. These reaction rate parameters must be focused on in field data monitoring scheme and in model parameter estimation.

HESSD
12, 1653–1696, 2015

3.5 Spatial distribution of parameter influence on C_{NO_3} and C_{O_2}

Cell-by-cell plots of Savage scores for the parameters according to their ranking in influencing C_{NO_3} in shallow groundwater are shown in Fig. 9. Plots are presented for each of the targeted 9 parameters except for $\lambda_{O_2}^{auto}$ due to the negligible influence of O_2 autotrophic reduction on C_{NO_3}. The value for each cell represents the ranking (1–9) and associated Savage score for the given parameter. High ranking in terms of influence is displayed in maroon-red coloring, whereas low ranking is displayed in blue. As seen in the plots, the ranking of each parameter in its influence on groundwater C_{NO_3} is highly spatially-variable. For example, the locations where $Canal_{NO_3}$ has the strongest influence (maroon coloring) (Fig. 9b) are scattered throughout the region, with in some cases entire local areas, encompassed by circles in Fig. 9b, governed by this parameter. For the cultivated areas, the dominant parameters (maroon-red coloring) are F_{NH_4} (Fig. 9a), N_{up} (Fig. 9d), and $\lambda_{NO_3}^{het}$ (Fig. 9e), with λ_H (Fig. 9g) having a moderate influence and λ_L (Fig. 9h) having a small influence. Whereas F_{NH_4} and N_{up} have the most influence on C_{NO_3} in most of the cultivated areas, some areas are governed principally by $\lambda_{NO_3}^{het}$ and λ_H (cells colored in maroon in Fig. 9e and g). Values of λ_H and λ_L control the rate of organic C and organic N decomposition and hence the availability of C for heterotrophic denitrification to proceed.

No area has λ_L being the dominant influence on C_{NO_3}. Nitrification rate of $NH_4\lambda_{nit}$ has a strong impact on C_{NO_3} in the Holbrook command area (red-pink cell coloring), with small impact elsewhere in the study area. $\lambda_{NO_3}^{auto}$ is the dominant parameter in areas along the Arkansas River and several of the tributaries (Fig. 9f) that are adjacent to shale formations (see Fig. 1). However, it is interesting to note that there are many locations in the study area adjacent to outcropped shale in which $\lambda_{NO_3}^{auto}$ is not the dominant parameter. These locations are indicated by circles in Fig. 9f. In these areas, other parameters such as F_{NH_4}, N_{up}, $\lambda_{NO_3}^{het}$ and λ_H are the governing influences on C_{NO_3},

HESSD
12, 1653–1696, 2015

demonstrating that knowledge of shale locations alone cannot be used to determine where C_{NO_3} will be affected the most by autotrophic denitrification.

Similar cell-by-cell plots of parameter Savage scores are shown in Fig. 10 for influence on C_{O_2} in shallow groundwater. λ_H and λ_L govern C_{O_2} in the cultivated areas (Fig. 10c and d), with F_{NH_4} (Fig. 10b), N_{up} (Fig. 10e) and $Canal_{NO_3}$ (Fig. 10a) exhibiting small to moderate influence on C_{O_2} in the cultivated areas. The strong influence of λ_H and λ_L occurs due to their control of the rate of organic C decomposition, and hence the availability of C for heterotrophic reduction of O_2. The rate of autotrophic reduction of $O_2\lambda_{O_2}^{auto}$ is dominant in localized areas where shale is present (see maroon-shaded cells in Fig. 10f) with small influences in other areas of the study region, mainly in areas down-gradient of the shale areas.

4 Summary and concluding remarks

This study used a 506 km^2 regional-scale N fate and transport numerical model to assess the influence of major forcing terms and chemical processes on NO_3 concentration in groundwater, NO_3 leaching from the unsaturated zone to the saturated zone of the aquifer, and NO_3 mass loading from the aquifer to the Arkansas River via groundwater discharge. Forcing terms include fertilizer loading, crop N uptake, and NO_3 concentration of applied irrigation water and canal seepage. Chemical processes include litter and humus organic N decomposition, nitrification of NH_4 to NO_3, heterotrophic and autotrophic reduction of NO_3, with the latter occurring in the presence of pyrite-bearing marine shale, and autotrophic reduction of O_2, also occurring in the presence of shale. The influence of each of the 9 model factors was computed using the revised Morris method for sensitivity analysis, with results processed to determine parameter influence globally for the entire study region, and specific to crop type, canal command area (i.e. the group of fields receiving irrigation water from a given canal), and individual grid cells. For the latter, spatial plots of sensitivity indices are presented to display the spatial distribution of influence for each model factor.

HESSD
12, 1653–1696, 2015

Results indicate that, generally, fertilizer loading, crop N uptake, and heterotrophic denitrification govern NO_3 mass transport, particularly in cultivated areas. However, their order of influence onand NO_3 mass leaching varies according to crop type and command area, and several command areas are influenced more, or at least to a significant degree, by nitrification, autotrophic denitrification, and. Spatial plots of cell-by-cell sensitivity indices further enhance the understanding of localized model factor influence, with each factor except for rate of heterotrophic O_2 reduction having the dominant influence overat one or more locations within the study area. Results also indicate that the concentration of O_2 in groundwater is governed by rates of organic matter decomposition, which releases CO2 and hence enhances heterotrophic reduction of O_2.

In general, the procedure followed in this study provides key information regarding overall NO_3 fate and transport in an agricultural groundwater system, guidance for future data collection and monitoring programs, an indication of which parameters should be targeted during model parameter estimation, and guidance for implementing best-management practices (BMPs) for NO_3 remediation, i.e. decreasing groundwater concentrations and NO3 mass loading to the stream network. For example, fertilizer loading, crop N uptake, andshould be targeted in field data collection and observation, withmonitored for each irrigation canal as often as possible, whereas first-order kinetic rate constants for nitrification, denitrification, and organic matter decomposition should be targeted during parameter estimation efforts. Furthermore, the procedure followed in this study also allows for data collection, management practice implementation, and parameter estimation to be performed on location-specific basis. For example, results suggest that a specific BMP (e.g., reduction in N fertilizer loading) may be optimal for several of the command areas but not for others, or that decreasingor the amount of NO3 denitrified in shale outcrop locations will help remediate NO_3 only in a few specific locations within the study area. Also, data collecting points for specific model factors can be restricted to sub-region areas, either to a given command area or, with the use of the spatial plots of sensitivity indices, to even more localized sites.

HESSD
12, 1653–1696, 2015

The Supplement related to this article is available online at doi:10.5194/hessd-12-1653-2015-supplement.

Acknowledgements. Financial support for this study was provided by grants from the Colorado Department of Public Health and Environment (03-00837, 05-00112, 05-00170, 09-00169, PO FAA WQC1349262), the Colorado Agricultural Experiment Station (COL00684), and the United States Bureau of Reclamation (99-FC-60-12140). The cooperation of numerous landowners in the LARV in providing access for field monitoring is greatly appreciated. The views and conclusions contained in this document are those of the authors and should not be interpreted as representing the opinions or policies of the government of Colorado or the US government. Data used in this study can be provided via a request to the corresponding author at rtbailey@engr.colostate.edu.

References

Almasri, M. N. and Kaluarachchi, J. J.: Modeling nitrate contamination of groundwater in agricultural watersheds, J. Hydrol., 343, 211–229, 2007.

Arabi, M., Govindaraju, R. S., Engel, B., and Hantush, M.: Multiobjective sensitivity analysis of sediment and nitrogen processes with a watershed model, Water Resour. Res., 43, W06409, doi:10.1029/2006WR005463, 2007.

Bailey, R. T. and Ahmadi, M.: Spatial and temporal variability of in-stream water quality parameter influence on dissolved oxygen and nitrate within a regional stream network, Ecol. Model., 277, 87–96, doi:10.1016/j.ecolmodel.2014.01.015, 2014.

Bailey, R. T., Hunter, W. J., and Gates, T. K.: The influence of nitrate on selenium in irrigated agricultural groundwater systems, J. Environ. Qual., 41, 783–792, 2012.

Bailey, R. T., Morway, E. D., Niswonger, R., and Gates, T. K.: Modeling variably saturated multispecies reactive groundwater solute transport with MODFLOW-UZF and RT3D, Groundwater, 51, 752–761, 2013a.

Bailey, R. T., Gates, T. K., and Halvorson, A. D.: Simulating variably-saturated reactive transport of selenium and nitrogen in agricultural groundwater systems, J. Contam. Hydrol., 149, 27–45, 2013b.

HESSD
12, 1653–1696, 2015

Bailey, R. T., Gates, T. K., and Ahmadi, M.: Simulating reactive transport of selenium coupled with nitrogen in a regional-scale irrigated groundwater system, J. Hydrol., 515, 29–46, 2014.
Birkinshaw, S. J. and Ewen, J.: Nitrogen transformation component for SHETRAN catchment nitrate transport modelling, J. Hydrol., 230, 1–17, 2000.
Cacuci, D. G.: Sensitivity and Uncertainty Analysis, Volume I: Theory, CRC Press, Boca Raton, Florida, 2003.
Campolongo, F. and Braddock, R., R.: Sensitivity analysis of the IMAGE Greenhouse model, Environ. Modell. Softw., 14, 275–282, doi:10.1016/S1364-8152(98)00079-6, 1999.
Campolongo, F. and Saltelli, A.: Sensitivity analysis of an environmental model: an application of different analysis methods, Reliab. Eng. Syst. Safe., 57, 49–69, doi:10.1016/S0951-8320(97)00021-5, 1997.
Campolongo, F., Cariboni, J., and Saltelli, A.: An effective screening design for sensitivity analysis of large models, Environ. Modell. Softw., 22, 1509–1518, doi:10.1016/j.envsoft.2006.10.004, 2007.
Chaplot, V., Saleh, A., Jaynes, D. B., and Arnold, J.: Predicting water, sediment and NO_3-N loads under scenarios of land-use and management practices in a flat watershed, Water Air Soil Poll., 154, 271–293, 2004.
Colorado Department of Public Health and Environment (CDPHE): "Regulation No. 31: The Basic Standards and Methodologies for Surface Water.", Denver, Colorado, 2012.
Conan, E., Bouraoui, F., Turpin, N., de Marsily, G., and Bidoglio, G.: Modeling flow and nitrate fate at catchment scale in Brittany (France), J. Environ. Qual., 32, 2026–2032, 2003.
Cox, B. A. and Whitehead, P. G.: Parameter sensitivity and predictive uncertainty in a new water quality model, Q^2, J. Environ. Eng.-ASCE, 131, 147–157, 2005.
Cukier, R., Fortuin, C. M., Schuler, K. E., Petschek, A. G., and Schaibly, J. H.: Study of the sensitivity of coupled reaction systems to uncertainties in rate coefficients. I Theory, J. Chem. Phys., 59, 3873–3878, 1973.
Deflandre, A., Williams, R. J., Elorza, F. J., Mira, J., and Doorman, D. B.: Analysis of the QUESTOR water quality model using a Fourier amplitude sensitivity test (FAST) for two UK rivers, Sci. Total Environ., 360, 290–304, 2006.
Ehteshami, M., Langeroudi, A. S., and Tavassoli, S.: Simulation of nitrate contamination in groundwater caused by livestock industry (cast study: Rey), J. Environ. Protection, 4, 91–97, 2013.

HESSD
12, 1653–1696, 2015

Fan, A. M. and Steinberg, V. E.: Health implications of nitrate and nitrite in drinking water: an update on methemoglobinemia occurrence and reproductive and developmental toxicity, Regul. Toxicol. Pharm., 23, 35–43, 1996.
Frind, E. O., Duynisveld, W. H. M., Strebel, O., and Boettcher, J.: Modeling of multicomponent transport with microbial transformation in groundwater: the Fuhrberg case, Water Resour. Res., 26, 1707–1719, 1990.
Gates, T. K., Cody, B. M., Donnelly, J. P., Herting, A. W., Bailey, R. T., and Mueller-Price, J.: Assessing selenium contamination in the irrigated stream-aquifer system of the Arkansas River, Colorado, J. Environ. Qual., 38, 2344–2356, 2009.
Hall, J. W., Tarantola, S., Bates, P. D., and Horritt, M. S.: Distributed sensitivity analysis of flood inundation model calibration, J. Hydraul. Eng.-ASCE, 131, 117–26, 2005.
Hall, J. W., Boyce, S. A., Wang, Y., Dawson, R. J., Tarantola, S., and Saltelli, A.: Sensitivity analysis for hydraulic models, J. Hydraul. Eng.-ASCE, 135, 959–969, doi:10.1061/(ASCE)HY.1943-7900.0000098, 2009.
Hefting, M. M. and de Klein, J. J. M.: Nitrogen removal in buffer strips along a lowland stream in the Netherlands: a pilot study, Environ. Pollut., 102, 521–526, 1998.
Holloway, J. M. and Dahlgren., R. A.:. Nitrogen in rock: occurrences and biogeochemical implications, Global Biogeochem. Cy., 16, 1118, doi:10.1029/2002GB001862, 2002.
Iman, R. L. and Conover, W. J.: A measure of top-down correlation, Technometrics, 293, 351–357, 1987.
Johnsson, H., Bergström, L., Jansson, P., and Paustian, K.: Simulated nitrogen dynamics and losses in a layered agricultural soil, Agr. Ecosyst. Environ., 18, 333–356, 1987.
Jørgensen, C. J., Jacobsen, O. S., Elberling, B., and Aamand, J.: Microbial oxidation of pyrite coupled to nitrate reduction in anoxic groundwater sediment, Environ. Sci. Technol., 43, 4851–4857, 2009.
Korom, S. F.: Natural denitrification in the saturation zone: a review, Water Resour. Res., 28, 1657–1668, 1992.
Lee, M., Park, G., Park, M., Park, J., Lee, J., and Kim, S.: Evaluation of non-point source pollution reduction by applying best management practices using a SWAT model and QuickBird high resolution satellite imagery, J. Environ. Sci., 22, 826–833, 2010.
Liu, D. and Zou, Z.: Sensitivity analysis of parameters in water quality models and water environment management, J. Environmental Protection, 3, 863–870, 2012.

HESSD
12, 1653–1696, 2015

Ma, L., Shaffer, M. J., Boyd, J. K., Waskom, R., Ahuja, L. R., Rojas, K. W., and Xu, C.: Manure management in an irrigated silage corn field: experiment and modeling, Soil Sci. Soc. Am. J., 62, 1006–1017, 1998.
McNab Jr., W. W. and Dooher, B. P.: Uncertainty analysis of fuel hydrocarbon biodegradation signatures in groundwater by probabilistic modeling, Ground Water, 36, 691–698, 1998.
Montross, G. G., McGlynn, B. L., Montross, S. N., and Gardner., K. K.:. Nitrogen production from geochemical weathering of rocks in southwest Montana, USA, J. Geophys. Res.-Biogeo., 118, 1068–1078, 2013.
Morris, M.: Factorial sampling plans for preliminary computational experiments, Technometrics, 33, 161–174, 1991.
Morway, E. D. and Gates, T. K.: Regional assessment of soil water salinity across an intensively irrigated river valley, J. Irrig. Drain. E.-ASCE, 138, 393–405, 2012.
Morway, E. D., Gates, T. K., and Niswonger, R. G.: Appraising options to enhance shallow groundwater table and flow conditions over regional scales in an irrigated alluvial aquifer system, J. Hydrol., 495, 216–237, 2013.
Niswonger, R. G., Prudic, D. E., and Regan, R. S.: Documentation of the unsaturated-zone flow (UZF1) package for modeling unsaturated flow between the land surface and the water table with MODFLOW-2005, US Geological Survey Techniques and Methods 6-A19, Reston, VA, USA, 2006.
Niswonger, R. G., Panday, S., and Motomu, I.: MODFLOW-NWT, a Newton formulation for MODFLOW-2005, US Geological Survey Techniques and Methods 6-A37, Reston, VA, USA, 44 p., 2011.
Ocampo, C. J., Sivapalan, M., and Oldham, C. E.: Field exploration of coupled hydrological and biogeochemical catchment responses and a unifying perceptual model, Adv. Water Resour., 29, 161–180, 2006.
Oyarzun, R., Arumí, J., Salgado, L., and Mariño, M.: Sensitivity analysis and field testing of the RISK-N model in the Central Valley of Chile, Agr. Water Manage., 87, 251–260, 2007.
Parkin, T. B. and Robinson, J. A.: Stochastic models of soil denitrification, Appl. Environ. Microb., 55, 72–77, 1989.
Reusser, D. E., Buytaert, W., and Zehe, E.: Temporal dynamics of model parameters sensitivity for computationally expensive models with the Fourier amplitude sensitivity test, Water Resour. Res., 47, W07551, doi:10.1029/2010WR009947, 2011.

HESSD
12, 1653–1696, 2015

Rong, Y. and Xuefeng, W.: Effects of nitrogen fertilizer and irrigation rate on nitrate present in the profile of a sandy farmland in Northwest China, Procedia Environ. Sci., 11, 726–732, 2011.
Sahu, M. and Gu, R. R.: Modeling the effects of riparian buffer zone and contour strips on stream water quality, Ecol. Engr., 35, 1167–1177, 2009.
Saltelli, A., Ratto, M., Andres, T., Campolongo, F., Cariboni, J., Gatelli, D., Saisana, M., and Tarantola, S.: Global Sensitivity Analysis. The Primer, John Wiley and Sons, West Sussex, UK, 2008.
Scott, G. R.: Geologic and structure contour map of the La Junta quadrangle, Colorado and Kansas , US Geological Survey, Reston, Virginia, 1968.
Sharps, J. A.: Geologic map of the Lamar quadrangle, Colorado and Kansas, US Geological Survey, Reston, Virginia, 1976.
Sincock, A. M., Wheater, H. S., and Whitehead, P. G.: Calibration and sensitivity analysis of a river water quality model under unsteady flow conditions, J. Hydrol., 227, 214–229, 2003.
Sobol', I. M.: Sensitivity analysis for non-linear mathematical models, Mathematical Modelling and Computational Experiment, 1, 407–414, 1993.
Spalding, R. F. and Exner, M. E.: Occurrence of nitrate in groundwater: a review, J. Environ. Qual., 22, 392–402, 1993.
Spruill, T. B.: Statistical evaluation of effects of riparian buffers on nitrate and ground water quality, J. Environ. Qual., 29, 1523–1538, 2000.
Sun, X., Newham, L., Croke, B., and Norton, J.: Three complementary methods for sensitivity analysis of a water quality model, Environ. Modell. Softw., 37, 19–29, doi:10.1016/j.envsoft.2012.04.010, 2012.
Vaché, K. B., Eilers, J. M., and Santelmann, M. V.: Water quality modeling of alternative agricultural scenarios in the U.S. Corn Belt, J. Am. Water Resour. As., 38, 773–787, 2002.
White, K. L. and Chaubey, I.: Sensitivity analysis, calibration, and validations for a multisite and multivariable SWAT model, J. Am. Water Resour. As., 41, 1077–1089, doi:10.1111/j.1752-1688.2005.tb03786.x, 2005.
Wriedt, G. and Rode, M.: Modelling nitrate transport and turnover in a lowland catchment system, J. Hydrol., 328, 157–176, 2006.
Wu, W.-M., Carley, J., Green, S. J., Luo, J., Kelly, S. D., Nostrand, J. V., Lower, K., Mehlhorn, T., Carroll, S., Boonchayanant, B., Löfller, F. E., Watson, D., Kemner, K. M., Zhou, J., Kitanidis, P. K., Kostka, J. E., Jardine, P. M., and Criddle, C. S.: Effects of nitrate on the stability

HESSD
12, 1653–1696, 2015

of uranium in a bioreduced region of the subsurface, Environ. Sci. Technol., 44, 5104–5111, 2010.

Zielinski, R. A., Asher-Bolinder, S., Meier, A. L., Johnson, C. A., and Szabo, B. J.: Natural or fertilizer-derived uranium in irrigation drainage: a case study in southeastern Colorado, USA, Appl. Geochem., 12, 9–21, 1997.

HESSD

12, 1653–1696, 2015

Table 1. Baseline agricultural management and crop parameter values for the model simulations.

Crop Type	Planting Day	Harvest Day	Plow Day	P_{St}	$d_{rt,\,max}$	CN_{RT}	F_{NH_4}	N_{up}
Units	–	–	–	kg ha^{-1}	m	–	kg ha^{-1}	kg ha^{-1}
Alfalfa	30 Apr	30 Sep	20 Oct	561.6	1.83	25	22.4	22.4
Bean	20 May	30 Sep	20 Oct	561.6	0.91	25	140	84.2
Corn	1 May	25 Oct	14 Nov	5616	1.22	70	252	224.6
Melon	15 May	10 Aug	30 Aug	561.6	1.22	25	112	112.3
Onion	20 Mar	15 Sep	5 Oct	561.6	0.46	25	140	78.6
Pasture	30 Aug	30 Sep	20 Oct	0	0.91	70	140	112.3
Pumpkin	1 Jun	30 Sep	20 Oct	561.6	0.91	25	140	84.2
Sorghum	20 May	15 Oct	4 Nov	1684.8	0.91	70	112	112.3
Spring Grain	1 Apr	15 Jul	4 Aug	1684.8	0.91	70	112	112.3
Squash	20 May	25 Jul	14 Aug	561.6	0.91	25	140	84.2
Sunflower	1 Jun	10 Oct	30 Oct	561.6	0.91	25	140	84.2
Vegetable	25 Apr	30 Aug	19 Sep	561.6	0.91	25	140	84.2
Winter Wheat	30 Sep	5 Jul	25 Jul	1684.8	0.91	70	112	112.3

d_{pw} (depth of plowing) is 1.0 m for all crops except beans (0.8 m).
P_{Rt} (seasonal mass of root mass) is 500 kg ha^{-1} for all crop types.
CN_{ST} (carbon : nitrogen ratio in stover mass) is 50 for all crop types.

HESSD
12, 1653–1696, 2015

Table 2. Parameters and values for chemical reactions involving organic matter decomposition, dissolved oxygen, and nitrogen species for the baseline simulation model.

Org. Matter Decomp.			Dissolved Oxygen			Nitrogen		
Param.	Value	Unit	Param.	Value	Unit	Param.	Value	Unit
λ_L	0.25	d^{-1}	$\lambda_{O_2}^{het}$	2.0	d^{-1}	$H_{C/N}$	12.0	–
λ_H	0.003	d^{-1}	$\lambda_{O_2}^{auto\,*}$	0.58	d^{-1}	$B_{C/N}$	8.0	–
f_e	0.5	–	K_{O_2}	1.0	$g\,m_f^{-3}$	I_{O_2}	1.0	$g\,m_f^{-3}$
f_h	0.2	–				λ_{nit}^{*}	0.98	d^{-1}
K_{CO_2}	0.75	$g\,m_f^{-3}$				λ_{vol}	0.1	d^{-1}
						$\lambda_{NO_3}^{het}$	0.1	d^{-1}
						$\lambda_{NO_3}^{auto\,*}$	0.22	d^{-1}
						K_{NO_3}	10.0	$g\,m_f^{-3}$
						K_{d,NH_4}	3.5	–

* Indicates mean value, with specific values assigned to each command area according to the values reported in Bailey et al. (2014).

HESSD
12, 1653–1696, 2015

Table 3. Sensitivity index (μ^*) for each of the model input factors investigated, indicating the degree of parameter influence on C_{NO_3} in the shallow saturated zone of the aquifer (in layer 4 of the grid) for the grid cells associated with each crop type and command area, with the values of the top three influential parameters for each crop type and command area bolded.

	F_{NH_4}	N_{up}	λ_L	λ_H	$\lambda_{O_2}^{auto}$	λ_{nit}	$\lambda_{NO_3}^{het}$	$\lambda_{NO_3}^{auto}$	$Canal_{NO_3}$
Crop									
Alfalfa	**0.46**	**0.56**	0.03	0.09	0.00	0.06	**0.23**	0.04	0.11
Bean	**0.70**	**0.43**	0.04	0.09	0.00	0.03	**0.34**	0.00	0.06
Corn	**0.94**	**0.72**	0.04	0.10	0.00	0.03	**0.30**	0.03	0.09
Melon	**5.46**	**3.02**	0.10	0.15	0.00	0.23	**0.92**	0.00	0.47
Onion	**1.21**	**0.99**	0.02	0.14	0.00	0.03	0.19	0.01	**0.45**
Pasture	**0.66**	**0.63**	0.03	0.12	0.01	0.04	**0.32**	0.07	0.14
Sorghum	**0.84**	**0.81**	0.03	0.12	0.00	0.08	**0.28**	0.04	0.13
Spring Grain	**0.79**	**0.70**	0.04	0.13	0.00	0.02	**0.32**	0.02	0.06
Command Area									
Catlin	**0.12**	**0.26**	0.00	0.03	0.01	**0.16**	0.04	0.01	0.11
Fort Lyon	**0.92**	**0.81**	0.05	0.17	0.00	0.04	**0.42**	0.08	0.12
Highline	**0.69**	**0.51**	0.03	0.06	0.00	0.02	0.23	0.01	**0.26**
Holbrook	**0.28**	**0.29**	0.02	0.03	0.00	0.01	0.08	**0.11**	0.10
Otero	**1.21**	**1.16**	0.05	0.14	0.00	0.04	0.49	0.04	**0.59**
RF Ditch	0.14	**0.15**	0.01	0.03	0.02	0.01	0.14	**0.20**	**0.51**

HESSD
12, 1653–1696, 2015

Table 4. Sensitivity index (μ^*) for each of the model input factors investigated, indicating the degree of parameter influence on NO_3 mass leaching from the shallow soil zone for the grid cells associated with each crop type and command area, with the values of the top three influential parameters for each crop type and command area bolded.

	F_{NH_4}	N_{up}	λ_L	λ_H	$\lambda_{O_2}^{auto}$	λ_{nit}	$\lambda_{NO_3}^{het}$	$\lambda_{NO_3}^{auto}$	$Canal_{NO_3}$
Crop Type									
Alfalfa	**395.9**	**613.7**	18.9	73.4	0.8	39.2	**176.2**	12.9	107.8
Bean	**42.8**	**25.6**	2.7	7.6	0.0	2.3	**22.3**	0.0	3.6
Corn	**486.3**	**366.8**	26.4	51.3	0.2	15.2	**172.3**	1.0	41.3
Melon	**7.0**	**4.5**	0.2	0.2	0.0	0.2	**1.9**	0.0	0.6
Onion	**9.7**	**7.2**	0.2	0.4	0.0	0.4	1.1	0.0	**1.6**
Pasture	**431.2**	**381.5**	15.7	76.2	0.4	9.0	**162.2**	11.6	49.0
Sorghum	**271.5**	**221.4**	10.6	28.8	0.1	10.9	**93.9**	2.1	26.2
Spring Grain	**213.5**	**179.3**	10.7	31.0	0.2	2.9	**81.7**	1.3	13.8
Command Area									
Catlin	**35.1**	**63.4**	0.9	5.3	0.1	**38.0**	7.5	0.3	9.2
Fort Lyon	**852.3**	**776.7**	34.5	140.1	1.0	33.4	**335.4**	13.1	70.0
Highline	**124.5**	**103.2**	4.2	11.7	0.0	2.7	**41.3**	0.1	36.7
Holbrook	**70.1**	**70.6**	3.6	5.7	0.1	2.6	**21.3**	3.6	10.4
Otero	**195.6**	**175.6**	8.4	20.9	0.0	4.7	**84.5**	2.0	62.0
RF Ditch	**3.6**	**3.9**	0.1	1.2	0.2	0.5	1.9	3.3	**30.3**

HESSD
12, 1653–1696, 2015

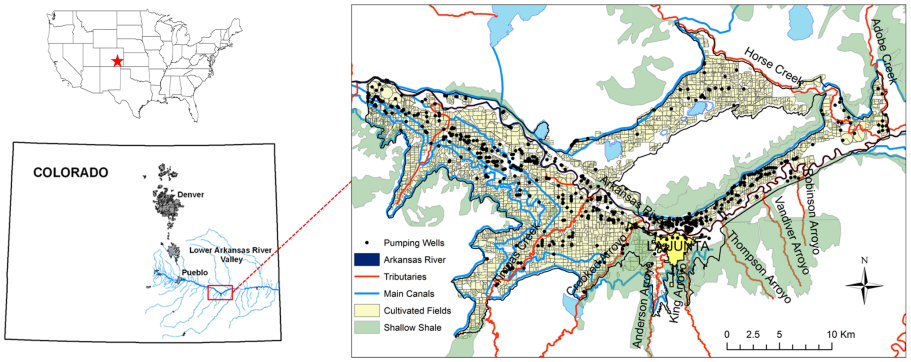

Figure 1. Location and hydrologic features of the study region in the Lower Arkansas River Valley in southeastern Colorado, showing the Arkansas River and tributaries (red), cultivated fields (yellow), irrigation canals (light blue), groundwater pumping wells (black dots), and the extent of near-surface shale (within 2 m of the ground surface) (green).

HESSD
12, 1653–1696, 2015

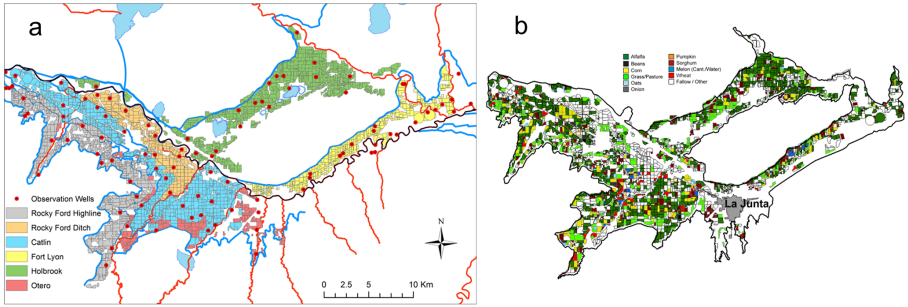

Figure 2. Features of the cultivation and data collection of the study region, including **(a)** canal command areas and location of groundwater observation wells, with a command area defined as the collection of fields receiving irrigation water from the same canal, and **(b)** the spatial distribution of crop cultivation during the 2006 growing season.

HESSD
12, 1653–1696, 2015

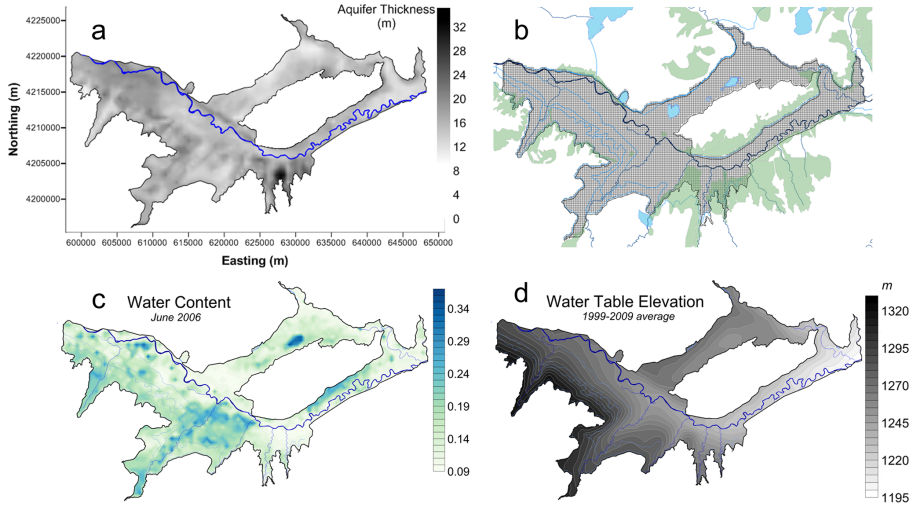

Figure 3. (a) The spatial distribution of aquifer thickness (m) of the alluvium in the study region, **(b)** the finite-difference grid used in the calibrated and tested MODFLOW-UZF1 groundwater flow model, using 250 m by 250 m grid cells, **(c)** spatial distribution of soil water content simulated by the MODFLOW-UZF1 model, for June 2006, and **(d)** average-simulated water table elevation for the 1999–2009 time period.

HESSD
12, 1653–1696, 2015

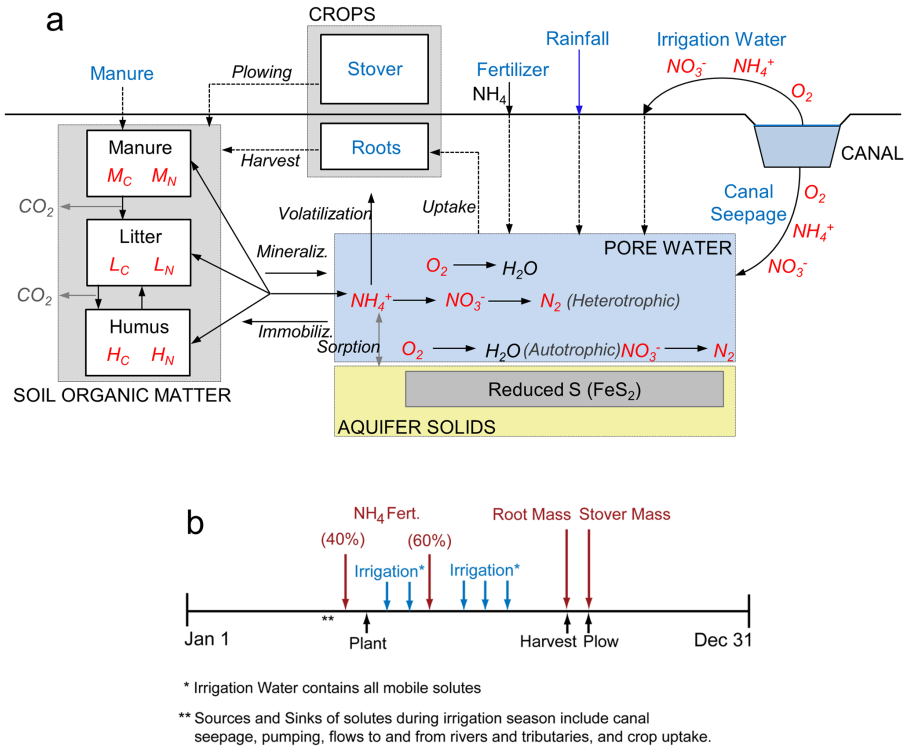

Figure 4. Depiction of the main processes simulated by the N reaction module of the UZF-RT3D model, with **(a)** conceptual model of the fate and transport of O_2 and N species in an irrigated soil-aquifer system wherein fertilizer, irrigation, and canal seepage bring solute mass into the subsurface environment, and **(b)** the annual cultivation schedule used in the N reaction module, including timing of planting, fertilizer loading, irrigation application, harvest, and plowing. NH_4 fertilizer has a split loading, with 40 % of the loading occurring 2 weeks before planting, and the remainder applied 6 weeks after planting.

HESSD
12, 1653–1696, 2015

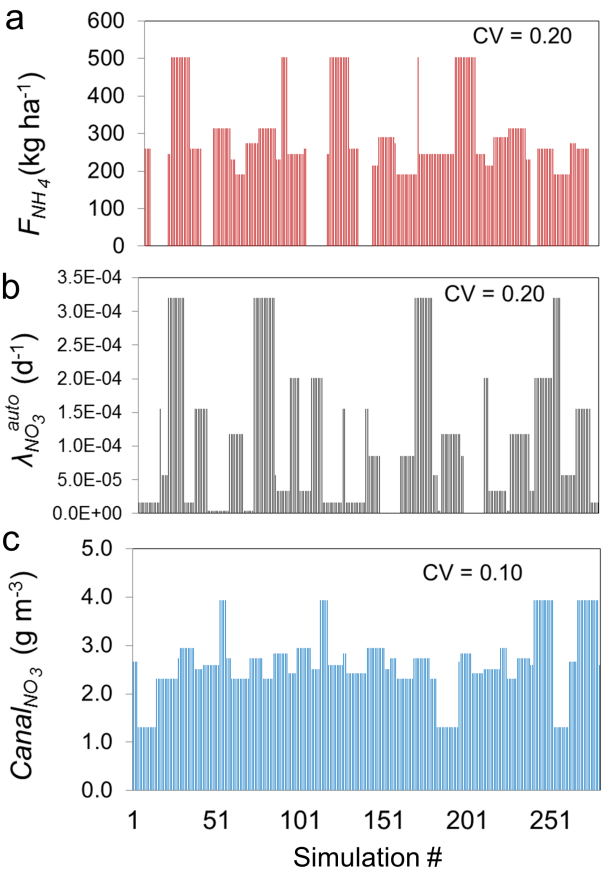

Figure 5. Values of **(a)** fertilizer loading F_{NH_4} (kg ha^{-1}) for corn, and **(b)** first-order rate constant of autotrophic denitrification $\lambda_{NO_3}^{auto}$ (day^{-1}) and **(c)** nitrate concentration of canal water $Canal_{NO_3}$ (mg L^{-1}) for the Rocky Ford Highline canal command area, for each of the 280 simulations in the revised Morris SA scheme.

HESSD
12, 1653–1696, 2015

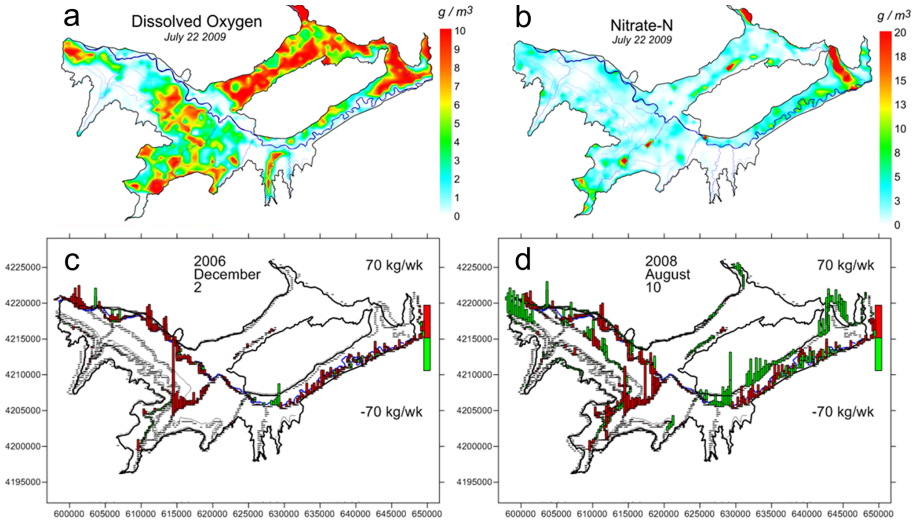

Figure 6. Summary of typical UZF-RT3D model results for the study region, showing spatial distribution of **(a)** C_{O_2} and **(b)** C_{NO_3} in shallow groundwater, and spatial distribution of mass loadings of nitrate to the Arkansas River system (main stem and tributaries) for **(c)** 2 December 2006, and **(d)** 10 August 2008, showing the contrast between the winter and summer seasons.

HESSD
12, 1653–1696, 2015

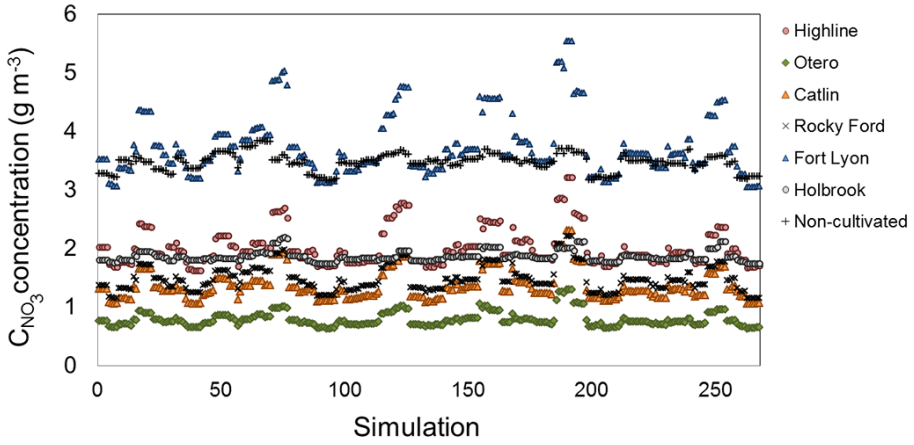

Figure 7. Spatio-temporal average value of C_{NO_3} in groundwater during the 2006–2009 simulation period for each canal command area for each of the 280 UZF-RT3D model simulations. The spatio-temporal average for the non-cultivated areas also is shown (small black crosses).

HESSD
12, 1653–1696, 2015

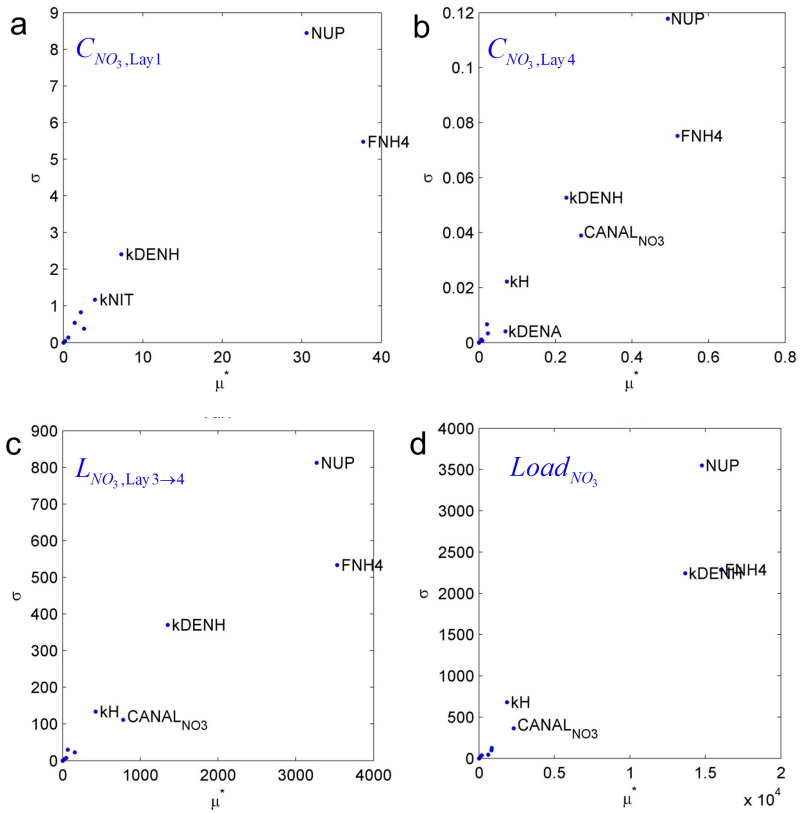

Figure 8. Global sensitivity plots (σ vs. μ^*) showing influence of the 9 targeted model input factors on **(a)** C_{NO_3} in Layer 1 of the model (top 0.5 m of the root zone), **(b)** C_{NO_3} in Layer 4 of the model (shallow saturated zone of the aquifer), **(c)** NO_3 mass leaching from Layer 3 to Layer 4 (unsaturated zone to saturated zone), and **(d)** total mass loading of NO_3 from the aquifer to the Arkansas River.

HESSD
12, 1653–1696, 2015

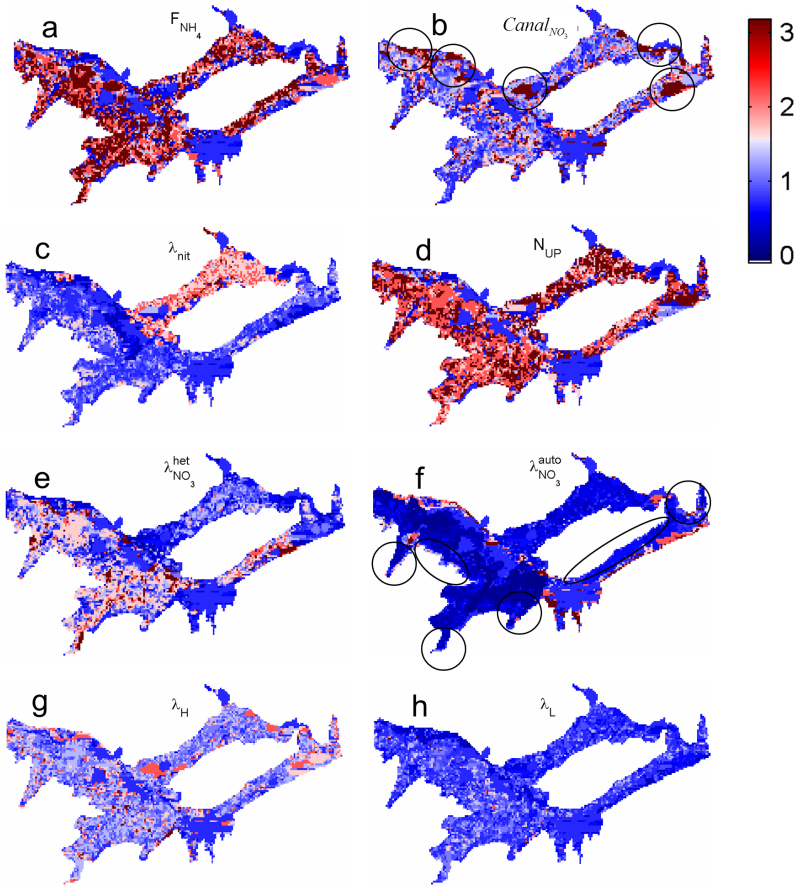

Figure 9. Cell-by-cell (250 m by 250 m) plots of Savage scores for **(a)** F_{NH_4}, **(b)** $Canal_{NO_3}$, **(c)** λ_{nit}, **(d)** N_{up}, **(e)** $\lambda^{het}_{NO_3}$, **(f)** $\lambda^{auto}_{NO_3}$, **(g)** λ_H, and **(h)** λ_L indicating the ranking of influence of that parameter on C_{NO_3} in groundwater for each of the 7776 cells in the study region.

HESSD
12, 1653–1696, 2015

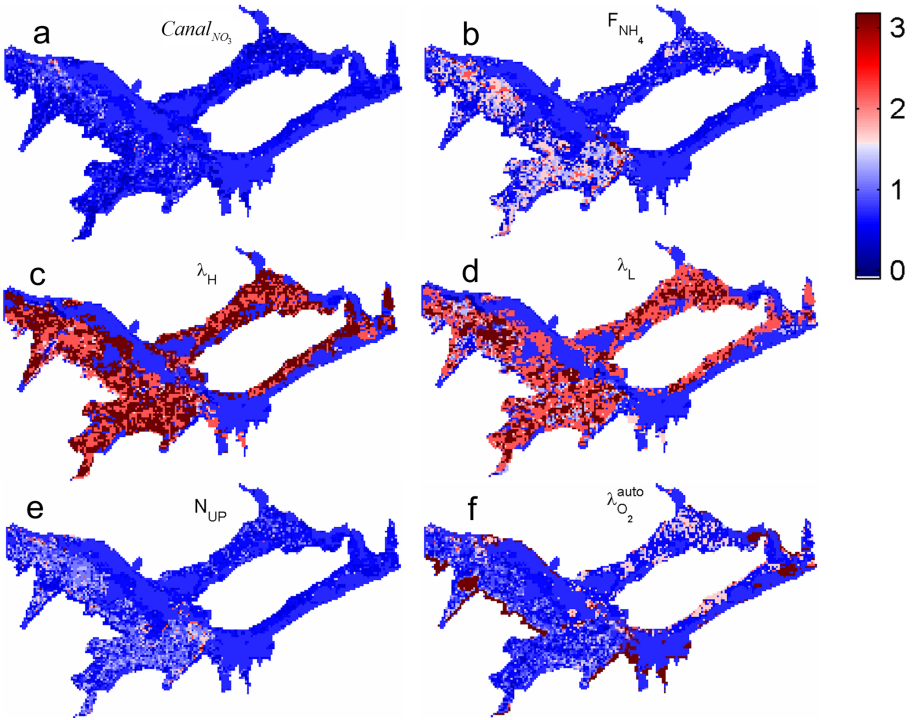

Figure 10. Cell-by-cell (250 m by 250 m) plots of Savage scores for **(a)** $Canal_{NO_3}$, **(b)** F_{NH_4}, **(c)** λ_H, **(d)** λ_L, **(e)** N_{up}, and **(f)** $\lambda^{auto}_{O_2}$, indicating the ranking of influence of that parameter on C_{O_2} in groundwater for each of the 7776 cells in the study region.

HESSD
12, 1653–1696, 2015